



## Research Paper

Upgrading HDS activity of MoS<sub>2</sub> catalysts by chelating thioglycolic acid to MoO<sub>x</sub> supported on alumina

José A. Toledo-Antonio\*, M.A. Cortes-Jacome, J. Escobar-Aguilar, C. Angeles-Chavez, J. Navarrete-Bolaños, E. López-Salinas

*Instituto Mexicano del Petróleo, Eje Central Lázaro Cárdenas # 152, Ciudad de México, 07730 Mexico*

## ARTICLE INFO

## Article history:

Received 13 February 2017

Received in revised form 11 April 2017

Accepted 2 May 2017

Available online 3 May 2017

## Keywords:

Hydrodesulfurization

Molybdenum sulfide

Thioglycolic acid

Chelating agent

Type II sites

## ABSTRACT

Alumina-supported Mo-based hydrodesulfurization catalysts (14 wt% nominal Mo loading) were modified by thioglycolic acid (TGA, TGA/Mo = 1 mol ratio), as a chelating agent containing a thiol group. To that end, two series of catalyst were prepared: the first one by using ammonium heptamolybdate as a precursor and, in the second one, *in situ* obtained phosphomolybdates from MoO<sub>3</sub> digestion in diluted H<sub>3</sub>PO<sub>4</sub>. Oxidic phases were characterized by N<sub>2</sub> physisorption, Raman and UV-vis spectroscopies, electron microscopy and XPS. As well, the corresponding sulfided phases were studied by XPS, HR-TEM-STEM techniques, and chemical composition was determined by STEM-EDX. Formation of ligand-to-metal charge transfer (LMCT) complexes between the S-bearing TGA and Mo atoms, resulted in reduced Mo<sup>5+</sup> species, as indicated by XPS, and was correlated to electronic transitions bands in the UV-visible spectra. On the other hand, the catalysts prepared from phosphomolybdates impregnation and TGA addition resulted in two-fold amount of Mo<sup>4+</sup> sulfided species, as indicated by XPS. TGA impregnation redissolve and disperse the MoO<sub>3</sub> resulting in materials particles in materials with increased stacking of MoS<sub>2</sub> slabs on which slabs length remained essentially unaltered. Highly active (as tested in liquid-phase dibenzothiophene hydrodesulfurization) Type II sites were favored mainly in sulfided TGA-modified formulations.

© 2017 Elsevier B.V. All rights reserved.

## 1. Introduction

Due to gradually scarce light crude oil reserves, low-quality heavy oils of higher concentration of atmospheric pollutants have to be used as raw materials in the production of ultra-low sulfur fuels. More efficient hydrodesulfurization (HDS) processes are consequently required. Strategies used on improving the related catalysts have been oriented mainly on enhancing dispersion and sulfidability of supported phases and in optimizing decoration of MoS<sub>2</sub> crystals by promoters (cobalt or nickel) as well.

Addition of chelating agents that could form a complex with Ni and Co promoters has been studied by various groups [1–4]. Commonly used chelating agents are ethylenediaminetetraacetic acid (EDTA) [1,4,5], nitrilotriacetic acid (NTA) [6,7] and citric acid (CA) [8,9], all of them containing carboxylic groups that chelate mainly the Co or Ni promoter and being typically added in the impregnating solution and after impregnation, catalysts are directly sulfided without calcination. Several investigations have been devoted to study the improvement of the HDS activity by the use of such

chelating agents and various explanations have been proposed. There is a general agreement that these complexes have to resist (e.g. not decompose) high temperature sulfiding, at least until reaching conditions at which Mo (or W) can be transformed to the corresponding sulfides. Organo-Co or –Ni species could be then thermally decomposed allowing promoters sulfidation and integration to Mo or W sulfides to produce highly active “CoMo(W)S” or “NiMo(W)S” phases [3,4]. Additionally, the beneficial role of citric acid as a modifier of Mo species-support interaction in sulfided CoMo/alumina catalysts on HDS performance has been recently emphasized [10]. In fact, chelating agents can also act as carbon source upon a sulfidation procedure, providing the following effects [11]: (i) a thermal effect, which modulate the exothermal sulfidation process, and a better control of MoS<sub>2</sub> crystallite growth; (ii) a geometrical effect, given that carbon deposits isolate the active sulfide crystallites stabilizing them against sintering; (iii) a support effect, since carbon species intercalated between the carrier and sulfide active phase reduce the interaction of the active MoS<sub>2</sub> phase with the support and enhance the HDS activity; and, (iv) a chemical effect, due to the formation of a more active carbide-like structure on the surface of the sulfide particles.

Addition of sulfur-bearing molecules, such as “alkylpolysulfides”, more specifically ditertiononyl pentasulfide (TNPS) have also

\* Corresponding author.

E-mail address: [jtoledo@imp.mx](mailto:jtoledo@imp.mx) (J.A. Toledo-Antonio).

been used for ex-situ sulfidation process generating presulfided HDS catalysts [12–14]. This procedure consists on the impregnation of TNPS on an oxidic phase of calcined HDS catalysts followed by hydrogen treatment at 150–350 °C at pressure up to 21 bar [13,14]. This method brings about a significant increase in catalytic activity as well as in the dispersion of active MoS<sub>2</sub> phase, in comparison with the corresponding HDS catalysts without TNPS addition [13,14]. Refiners prefer this method, since it produces pre-sulfided catalysts that reduce start-up time from days to hours, minimize an out-of-specification product, and eliminate dangerous sulfur agents and their handling [15]. On the other hand, besides the regeneration procedure, which removes coke deposits in soft oxidizing conditions, additional treatments are required in order to recover the catalysts properties. These treatments typically consist in exposing the de-coked catalysts with some chemical compounds, for instance some oxygen containing compounds, playing the role of chelating agents, which re-disperse the metals agglomerated upon regeneration [16].

Even though S-containing thioglycolic acid (TGA) has shown interesting properties as complexing agent on HDS catalyst preparation, just a few reports have dealt with TGA's beneficial effects [17–19]. Blanchard et al. [17] found that TGA could chelate both Co and Mo and that it could be then simultaneously liquid-phase sulfide, thus providing efficient control of the highly active "CoMoS" phase formation. On the other hand, in catalysts activated by gas-phase sulfiding [18], TGA addition resulted in both increased sulfidation degree of both Co and Mo and shorter length of corresponding slabs by efficient integration of cobalt to MoS<sub>2</sub> edges; e.g. increasing the amount of decorating Co and favoring CoMoS phase formation.

More recently, it was found that the preparation step where TGA was mixed with Ni and Mo, was crucial in terms of HDS activity of corresponding sulfide materials [19]. TGA effect on properties of Nb-HMS-supported NiMo depended on the stage at which TGA was added; being negative when added on the calcined material, or being slightly deleterious when simultaneously deposited along NiMo precursors. Also, by changing the support from Nb-HMS to Nb SBA-15 [19], TGA influence over sulfide NiMo phases was strongly modified; being good when added on calcined materials and, being excellent when simultaneously impregnated with NiMo precursors.

Here in, we propose to use TGA as a chelating agent since it contains both –SH and –COOH groups, the carboxylic group is typical of chelating EDTA, or citric acid or NTA, and the sulfide group is characteristic of alkylpolysulfides. Then, TGA can be added either to the impregnation solution to chelate both promoter and Mo species or to oxidic phases of HDS catalysts. Addition of TGA over oxidic phases of HDS catalyst could provide an ex-situ sulfidation and/or a rejuvenation/reactivation procedures as reported previously for alkylpolysulfides.

A better understanding on the TGA effect on the properties of supported molybdenum HDS catalysts is clearly needed. This work focuses on determining the influence of chelating TGA additive when impregnated (TGA/Mo = 1) on calcined (500 °C) alumina-supported molybdenum materials. The catalysts were characterized through various instrumental techniques attempting to explain the activity trend found in liquid-phase dibenzothiophene HDS in batch reactor at conditions close to those used in industrial units of diesel fuel production.

## 2. Experimental

### 2.1. Catalysts preparation

Pseudobohemite, Versal 250 from Eurosulphor, was used as a carrier, calcined at 550 °C for 6 h, to transform it into

gamma-alumina powder with a specific surface area of 283 m<sup>2</sup>/g. Molybdenum precursors were impregnated on gamma-alumina powder (14 wt% Mo nominal loading) by incipient wetness through two different methods. In the first one (Mo/Al sample), ammonium heptamolybdate (AHM) was dissolved in doubly distilled water (final solution pH = 5.6), the volume of distilled water used was determined by the pore volume of the carrier. The aqueous solution containing AHM was poured into gamma-alumina powder and the resulting paste being aged at room temperature for 18 h, then, dried at 120 °C overnight. In the second method (MoP/Al sample), the impregnating solution was prepared by digesting an appropriate amount MoO<sub>3</sub> (14 wt% Mo nominal loading in the final solid) with phosphoric acid (1.5 wt% P nominal loading) at 95 °C in excess water (300 ml). After several hours of reflux, the solution was concentrated to a volume equivalent to that of the pores of the support to be impregnated (final pH ~ 1.8). Further processing included aging and drying at 120 °C, similar to the case of the first preparation. Both dried samples were calcined at 500 °C under an air flow (0.6 l/h/g) for 4 h. Each sample was then divided into two equal portions, one of them being modified by TGA impregnation (at TGA/Mo = 1 molar ratio) through corresponding aqueous solutions. Finally, the solids impregnated with the organic acid (TGA/Mo/Al and TGA/MoP/Al) were dried at 80 °C overnight; high-temperature calcining being avoided to preserve organo-S modifier integrity.

### 2.2. Catalysts characterization

Textural properties were measured in an ASAP-2000 analyzer from Micromeritics. Specific surface area (SSA) was calculated from N<sub>2</sub> physisorption at -196 °C using the Brunauer-Emmet-Teller (BET) equation. Average pore size was obtained by the Barrett-Joyner-Halenda(BJH) method from desorption branch data. Materials ex situ calcined at 550 °C were outgassed at 350 °C prior to corresponding analysis.

Raman spectra were obtained using a Yvon Jobin Horiba (T64000) spectrometer, equipped with a CCD camera detector. As a source of excitation the 514 nm line of a Spectra Physics 2018 Argon/Krypton Ion Laser system was focused through an Olympus BX41 microscope equipped with a 100X magnification objective. The laser power never exceeded 5 mW on the sample.

A Perking Elmer lambda 900 UV-vis spectrometer equipped with an integrating sphere was used to record diffuse reflectance spectra (DRS). Spectralon® was used as reference material. All spectra were acquired at room temperature over fine powdered samples (without any pre-treatment) ex-situ dried at 80 °C. Corresponding spectra were deconvoluted into their main components by using Gaussian functions with satisfactory fitting in all cases.

X-ray photoelectronic spectroscopy (XPS) on sulfide catalysts was determined in a THERMO-VG scalab 250 spectrometer equipped with AlK<sub>α</sub> X-ray source (1486.6 eV) and a hemispherical analyzer. Experimental peaks were deconvoluted into single components using mixed Gaussian-Lorentzian functions and non-linear squares fitting algorithm, and applying Shirley background subtraction. Area ratio of 2/3 and splitting of 3.2 eV were used to fit the Mo 3d peaks. Binding energies were reproducible within ±0.2 eV and the C 1 s peak at 284.6 eV was used as a reference from adventitious carbon. Surface elemental composition was determined by fitting and integrating the Mo 3d, S 2p, O 1s and Al 2p bands and converting those values to corresponding atomic ratios using theoretical sensitive factors provided by the XPS apparatus manufacturer. All XPS curves are shown with the differential fitting curve (bottom curve in each spectrum) after adjusting to theoretical ones. All manipulation of sulfide samples was done under inert conditions in a glove-box and a special box vessel attached to the XPS equipment to introduce samples into the spectrometer's ultra-high vacuum chamber.

High-resolution Transmission electron microscopy (HR-TEM) was performed in a JEM-2200FS microscope with 200 kV accelerating voltage. The microscope was equipped with a Schottky-type field emission gun and ultra-high resolution configuration ( $C_s = 0.5$  mm;  $C_c = 1.1$  mm; point-to-point resolution = 0.19 nm) and in-column omega-type energy filter. STEM images were acquired in high angle annular dark-field (HAADF) mode using a cold-field emission JEOL ARM200CF operating at 200 kV and equipped with CEOS aberration correction for the probe-formation. In the HAADF mode, bright contrast images of the atomic column positions can be acquired. The images are dominated by the Z-contrast, namely the intensity is approximately proportional to  $Z^2$  (Z being atomic number).

Samples of catalytic solids were ground, suspended in isopropanol at room temperature and dispersed under ultrasonic stirring. Then, drops of the solution were put on a 3 mm diameter lacey-carbon copper grid. Average length and stacking number of  $\text{MoS}_2$  slabs ( $L_{\text{avg.}}$  and  $N_{\text{avg.}}$ , respectively) were statistically estimated [20] through measurements carried out in 120–130 crystallites per sample through the following equations:

$$L_{\text{avg.}} = \frac{\sum n_i L_i}{\sum n_i} \quad (1)$$

$$N_{\text{avg.}} = \frac{\sum n_i N_i}{\sum n_i} \quad (2)$$

where  $n_i$  is the number of slabs in a given range of length or stacking ( $L$  and  $N$ , respectively) and  $t$  is the total number of analyzed  $\text{MoS}_2$  slabs.

### 2.3. HDS catalytic test

To obtain active sulfide catalysts, sulfidation of oxidic samples was carried out at 380 °C, under a 10 vol.%  $\text{H}_2\text{S}/\text{H}_2$  flow for 2 h. This step was done in a tubular down-flow Pyrex glass reactor, the  $\text{H}_2\text{S}/\text{H}_2$  mixture being fed at a 24 l/h constant flow rate. This routine is standard in activating HDS catalysts [21,22].

Sulfided catalysts (~0.2 g) were tested in HDS of dibenzothiophene (DBT, ~0.3 g), model compound, representing S-bearing compounds in middle distillates, in a SS316 batch reactor using *n*-hexadecane (100 ml) as solvent (initial DBT concentration was 16.3  $\mu\text{mol/L}$ , 674 ppm S). The reaction temperature was 320 °C at a stirring rate of 1000 rpm. After operating temperature was attained,  $\text{H}_2$  (Ultra High Purity) was fed to the reactor to get 5.5 MPa (total pressure). Samples of liquid product were analyzed in a Varian 3400 CX gas chromatograph, equipped with a flame ionization detector and dimethylpolysiloxane (50 m  $\times$  0.2 mm  $\times$  0.5  $\mu\text{m}$ ) capillary column. HDS kinetic constants ( $k$ ) were calculated assuming pseudo-first order kinetics referred to DBT concentration ( $x$  = conversion,  $t$  = time), taking into account that hydrogen was fed in such excess that its partial pressure can be considered constant:

$$k = \frac{-\ln(1-x)}{t} \quad (3)$$

$k$  values for various catalysts were normalized by considering reaction volume and mass of catalyst used. Then, these values were adjusted by Mo loading in various tested formulations ( $k$  in  $1/(g_{\text{Mo}} \text{s})$ ).

**Table 1**

Textural properties of alumina support and oxidic impregnated materials (calcined at 500 °C).

Material	SSA ( $\text{m}^2/\text{g}$ )	$V_p$ ( $\text{cm}^3/\text{g}$ )	$D_p^a$ (nm)
$\text{Al}_2\text{O}_3$	283	0.89	12.6
Mo/Al	252	0.74	11.7
MoP/Al	218	0.71	13.0

<sup>a</sup> From  $4 \times V_p/\text{SSA}$ .

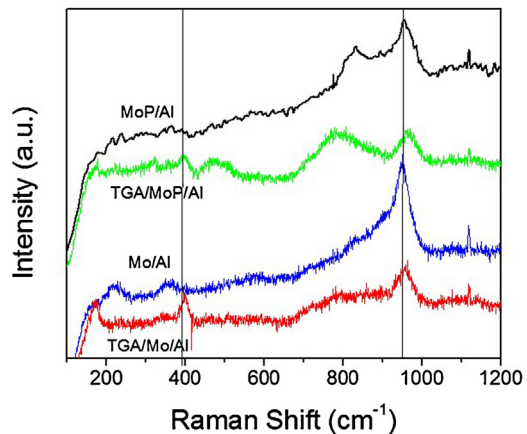


**Fig. 1.** Raman spectra of oxidic Mo/Al and MoP/Al catalysts prepared with and without TGA as indicated.

## 3. Results and discussion

### 3.1. Textural properties

Surface area, pore volume and average pore diameter (SSA,  $V_p$  and  $D_p$ , respectively), of alumina support and supported Mo-impregnated oxides are shown in Table 1. A lower SSA and  $V_p$  of Mo-catalysts (14 wt% nominal loading) was observed on corresponding oxides suggesting that oxidic molybdenum species dispersed on the alumina support occupy the void space in the pores.

Lower textural properties of MoP/Al compared to those of Mo/Al nicely corresponded to deposition of larger  $\text{MoO}_x$  aggregates as will be discussed in the following sections, additionally, the MoP/Al sample contains 1.8 wt% (determined by EDS) of phosphorous that correspond to ~4.1 wt% of phosphorus pentoxide.

### 3.2. Raman spectroscopy

Raman Spectra of the Mo/Al and MoP/Al samples prepared with and without TGA are shown in Fig. 1. The Mo/Al sample had vibrating bands at 220, 345–360 and 950  $\text{cm}^{-1}$ . These Raman signals are typical for Mo oxide supported catalysts. According to the literature [23,24] the signal at 950  $\text{cm}^{-1}$  can be attributed to Mo=O bonds asymmetric stretching in hydrated tetrahedral Mo oxide on alumina, whereas signals at 218 and 345–360  $\text{cm}^{-1}$  arise from rotational of rigid  $\text{MoO}_4$  chains and to O–Mo–O scissoring and bending vibrating modes, respectively [25]. The intensity of the former signal suggested abundant terminal Mo=O moieties that could be related to highly dispersed species. A broad band between 800 and 900  $\text{cm}^{-1}$ , can be attributed to symmetric MoO stretching, ruling out the presence of surface polymolybdates.

On the other hand, Raman spectrum of MoP/Al sample was made up of bands at 830 and 955  $\text{cm}^{-1}$  from MoO stretching symmetric and asymmetric vibrations, respectively, in polymolybdate species or  $\text{MoO}_x$  nanoparticles. The intense 830  $\text{cm}^{-1}$  signal characteristic of large  $\text{MoO}_3$  aggregates, suggest that impregnation with phos-

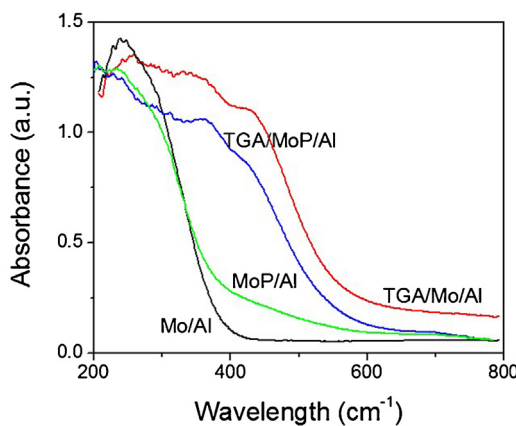


**Fig. 2.** Diffuse reflectance UV-vis spectra of oxidic Mo/Al and MoP/Al catalysts prepared with and without TGA, as indicated.

phomolybdates solution inhibited at some extent the interaction of  $\text{MoO}_x$  species with the carrier, thus yielding larger aggregates of polymolybdates or  $\text{MoO}_x$  species. Bands at 215 and 240  $\text{cm}^{-1}$ , also observed in Mo/Al, appeared in MoP/Al too, but with lower intensity [25]. Other two less intense vibrations appeared at 366 and 343  $\text{cm}^{-1}$ , which are from scissoring and bending vibrations of  $\delta$  O-Mo-O bonds, respectively [25].

TGA addition on Mo/Al and MoP/Al samples resulted in a band at 396  $\text{cm}^{-1}$  from vibrations of Mo-S bond,s presumably originated by surface reaction of polymolybdates with sulfur-bearing TGA. Accordingly, Payen et al. [18] found similar vibrating bands in samples modified by thioglycolic acid (at TGA/Mo = 4) attributing that to Mo-TGA complexes formation. Intensity of characteristic stretching bands of Mo=O of well-dispersed polymolybdate species (at 950 and 955  $\text{cm}^{-1}$  for Mo/Al and MoP/Al, respectively) was significantly lower in comparison with that in Raman spectra of samples without TGA (see Fig. 1). According to Blanchard et al. [17], these bands in TGA-modified Mo/alumina samples are an indication of some non-complexated molybdenum species. Also, the blue-shift observed for these bands in TGA-modified samples suggests Mo=O bonds shortening due to dehydration. Indeed, similar shifts have been related to change from molybdenyl sites in polymolybdate clusters to isolated mono-oxo sites [26]. That is, unstable clusters, lacking coordinating oxygen atoms after OH-groups elimination, might break down. That is a strong indication to Mo species redispersion by TGA addition. A very broad band at 780  $\text{cm}^{-1}$ , which is more clearly distinguishable in TGA/MoP/Al, can be attributed to reduced Mo<sup>V</sup>-OH species [27].

### 3.3. UV-vis diffuse reflectance spectroscopy

Diffuse reflectance UV-vis spectroscopy was used to examine the coordination environment of Mo species with TGA on Mo/Al and MoP/Al catalysts. In both TGA-modified samples, the spectra were considerably red-shifted in comparison with those prepared with no organic additive, due to ligand to metal charge transfer (LMCT) between the S-bearing compound and Mo atoms. Moreover, the bathochromic shift was stronger in the case of the solid prepared in presence of phosphates, pointing out to a stronger interaction of deposited Mo with TGA. Indeed, two intense bands in the visible region and reversible electron-transfer behavior have been observed in spectra of complexes of partially reduced molybdenum and S-bearing chelating compounds [28]. Accordingly, TGA coordinates with molybdenum by chelating the metal via the -SH and -COOH groups. For TGA-modified supported NiMo materials other authors [19] have found signals in the visible region between 550 and 600 nm attributing them to Mo- and/or Ni-TGA complexes for-

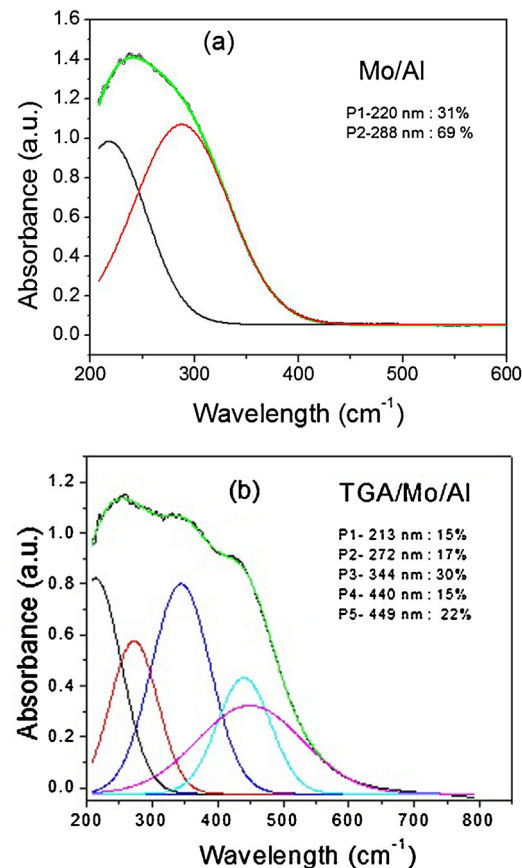


**Fig. 3.** Deconvoluted diffuse reflectance UV-vis spectra of: (a) Mo/Al and (b) TGA/Mo/Al catalysts prepared with and without TGA.

mation. However, the identification of these absorptions was done in samples where Ni, Mo and TGA (TGA/Mo = 4) were simultaneously impregnated over Nb-modified SBA-15 and HMS silica-based carriers. Differently to our case, they did not observe the aforementioned signals in the case of solids where the organic chelator was deposited on the corresponding calcined (500 °C) materials. In our study, aqueous solutions of TGA (in equimolar concentration regarding Mo loading) were added to tetrahedral  $\text{MoO}_4^{2-}$  and octahedral  $\text{MoO}_6^{2-}$  (isolated and/or in polymolybdate species stabilized on the alumina support). Then, the type of carrier used could also affect complexes formation.

In order to estimate the amount Mo species dispersed on the  $\text{Al}_2\text{O}_3$  carrier, UV-vis spectra from various samples were deconvoluted (see Figs. 3 and 4). In the case of the Mo/Al solid (Fig. 3a), UV-vis spectrum was made up of two absorption peaks with maxima at 220 and 288 nm. As energy of electron transitions depend on the ligand field symmetry around the Mo center, for oxygen ligands a more energetic transition is expected for tetrahedral (*Td*)  $\text{Mo}^{\text{VI}}$  than for octahedral ones [29]. Then, the peak at 220 nm is likely due to LMCT of  $\text{O}^{2-}$  to  $\text{Mo}^{\text{VI}}(\text{d}^0)$  in  $(\text{MoO}_4)^{2-}$  in *Td* symmetry [29], whereas the one at 288 nm corresponded to LMCT of  $\text{O}^{2-}$  to  $\text{Mo}^{\text{VI}}(\text{d}^0)$  of  $\text{MoO}_6$  in octahedral symmetry, in monomeric and/or polymolybdate species, respectively.

On the other hand, the UV-vis spectrum of MoP/Al sample (Fig. 4a) was fitted with three peaks at 204, 296 and 329 nm. The former two corresponded to LMCT of  $\text{O}^{2-}$  to  $\text{Mo}^{\text{VI}}$  species in tetrahedral and octahedral (polymeric) coordination, respectively, whereas the latter one can be associated to corresponding charge transfer in  $\text{MoO}_3$  clusters or aggregates [29]. These results are in agreement with those of Raman spectroscopy (see Fig. 1), where

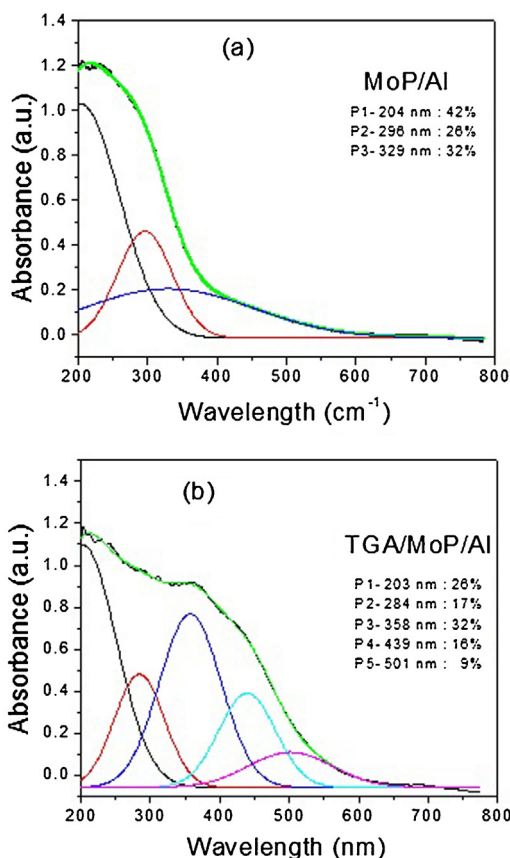


**Fig. 4.** Deconvoluted diffuse reflectance UV-vis spectra of: (a) MoP/Al and (b) TGA/MoP/Al catalysts prepared with and without TGA.

larger domains of more polymerized species where identified in MoP/Al, in comparison with those on Mo/Al.

UV-vis spectra of TGA/Mo/Al and TGA/MoP/Al samples were fitted with five contributions each one (Fig. 3b and 4b, respectively). In the former solid the deconvoluted peaks were at 213, 272, 344, 440, and 449 nm, whereas those in the latter were located at 203, 284, 358, 439 and 501 nm. As previously mentioned, the former two contributions corresponded to LMCT of O<sup>2-</sup> to Mo<sup>VI</sup> in isolated tetrahedral MoO<sub>4</sub><sup>2-</sup> and octahedral MoO<sub>6</sub><sup>2-</sup> in polymolybdate species. These contributions appeared at lower wavelength (so, at higher energy) in samples with TGA, suggesting a less-distorted tetrahedral MoO<sub>4</sub><sup>2-</sup> and octahedral MoO<sub>6</sub><sup>2-</sup> species [29]. The three peaks at longer wavelength (344–358, 439–440, and 449–501) may correspond to the formation of metalorganic complexes of Mo and TGA. In fact, numerous reactions of molybdates with organo-sulfur compounds in aqueous phase have been reported in literature. For instance, the reaction of cysteine (CH<sub>2</sub>(SH)CH(NH<sub>2</sub>)COOH) with Mo<sup>VI</sup> and Mo<sup>V</sup> take place through interaction between the ionized mercapto- and either the amino or carboxyl group [30]. In Mo<sup>VI</sup> the reaction may occur on various metal:ligand ratios, from 1:3 to 1:1, whereas with Mo<sup>V</sup> only the 1:1 complex formed; the Mo<sub>2</sub>O<sub>3</sub>(xanthate)<sub>4</sub> structure being proposed in this instance [30]. TGA oxidation by Mo<sup>VI</sup> and Mo<sup>V</sup> in aqueous solution with a phosphate buffer has also been investigated [31]. In the former case, reaction of Mo<sup>VI</sup> with TGA proceeded in two stages: first, reduction of Mo<sup>VI</sup> to a dimeric Mo<sup>V</sup>-TGA complex, then to stable Mo<sup>IV</sup> species of undetermined structure [31]. The structure of the intermediate complex was Mo<sup>VI</sup>O<sub>2</sub>(TGA)<sub>2</sub><sup>2-</sup> and Mo<sup>V</sup><sub>2</sub>O<sub>3</sub>(TGA)<sub>4</sub><sup>4-</sup>, where in both cases metal:ligand ratio 1:2 was used. The slightly higher absorption background of TGA/Mo/Al sample can be related to its brownish-yellow color.

**Table 2**

Binding energy values for surface Al, Mo, P and S species over various as prepared materials, from analysis and deconvolution of XPS spectra of Fig. 5. Full-width at half maximum (FWHM) values of various signals also included (in parentheses). Mo<sub>T</sub> = Mo<sup>VI</sup> + Mo<sup>V</sup>.

Sample/signal assignment	Al 2p	Mo <sup>VI</sup> 3d <sub>5/2</sub>	Mo <sup>V</sup> 3d <sub>5/2</sub>	P 2p	S 2p	Mo <sup>V</sup> /Mo <sub>T</sub>
Mo/Al	73.6 (2.1)	232.6 (2.3)				
MoP/Al	74.5 (2.1)	233.0 (2.3)		134.2 (2.4)		
TGA/Mo/Al	74.1 (2.1)	232.3 (2.0)	230.5 (2.1)		162.5 (3.2)	0.38
TGA/MoP/Al	74.1 (2.1)	232.8 (1.6)	231.5 (2.9)	133.5 (2.5)	163.0 (2.1)	0.78

In our study, aqueous solutions of TGA were added to tetrahedral MoO<sub>4</sub><sup>2-</sup> and octahedral [MoO<sub>6</sub>]<sup>2-</sup> (isolated and/or in polymolybdate species stabilized on the alumina support) to identify and characterize the different Mo-TGA surface complexes formed. Charge-transfer interactions of different energy were expected to occur in various surface Mo-TGA complex. According to literature, the UV-vis absorption peak at 344–358 cm<sup>-1</sup> can be assigned to Mo<sup>V</sup><sub>2</sub>O<sub>3</sub>(TGA)<sub>4</sub><sup>4-</sup> complex [31], whereas the other two absorption peaks at 439–440, and 449–501 cm<sup>-1</sup> likely correspond to Mo<sup>VI</sup>O<sub>2</sub>(TGA)<sub>2</sub><sup>2-</sup> and Mo<sup>VI</sup>O(TGA)<sup>-</sup> complexes, respectively. Nevertheless, a DFT calculation of the different proposed complexes are required to assign unambiguously the UV-vis absorption peaks.

### 3.4. XPS analysis of oxidic catalysts precursors

Mo 3d signals of oxidic samples without TGA were fitted assuming only one molybdenum oxidation state. Two signals at 232.6–233.0 and 235.8–236.2 eV (Mo 3d<sub>5/2</sub> and Mo 3d<sub>3/2</sub>, respectively) characteristic of Mo<sup>VI</sup> species [18] were identified in the spectra of both Mo/Al and MoP/Al materials (see Fig. 5a and b, respectively, and the corresponding XPS parameters in Table 2). After TGA impregnation, two new Mo species were necessary to fit the XPS spectra (see Fig. 5c and d). The first one, with Mo 3d<sub>5/2</sub> signals at 232.3–232.8 eV may be related to Mo<sup>VI</sup> of MoO<sub>x</sub> domains, whereas the second one with Mo 3d<sub>5/2</sub> signal at 230.5–231.5 eV corresponded to partially reduced Mo<sup>V</sup>, originated by LMCT in complexes between TGA and MoO<sub>x</sub> species [32]. Additionally, the XPS peak at 227.5 eV originated from the 2s signal of sulfur atoms in TGA [18(7)]. Noteworthy, The Mo<sup>V</sup> fraction was higher when TGA was impregnated over MoP/Al, in comparison with that on Mo/Al sample (Table 2). As indicated by Raman and UV-vis spectroscopies (see Figs. 1 and 2, respectively), larger aggregates of surface MoO<sub>x</sub> species were dispersed when phosphomolybdates were impregnated on alumina (MoP/Al solid), pointing out to inhibition of strong interactions of MoO<sub>x</sub> species with the alumina surface due to phosphorus addition. The LMCT complexes formation by TGA addition resulted in partial reduction of Mo<sup>VI</sup> to Mo<sup>V</sup> species. A larger proportion of the latter on MoP/Al strongly suggest that a higher amount of LMCT complexes formed by an extensive interaction of the organic modifier with larger MoO<sub>x</sub> aggregates present on that sample. The identification of Mo<sup>VI</sup> and Mo<sup>V</sup> oxidation states on TGA-modified samples indicated that Mo was partially reduced, in agreement with corresponding Raman spectrum in Fig. 1. The amount of reduced Mo<sup>V</sup> in TGA/MoP/Al was similar to that found by Payen et al. [18] for TGA-modified CoMo/alumina sample at much higher organic agent content (TGA/Mo=4) suggesting that a significantly weaker Mo-support interaction due to phosphate deposition, facilitated Mo complexes formation.

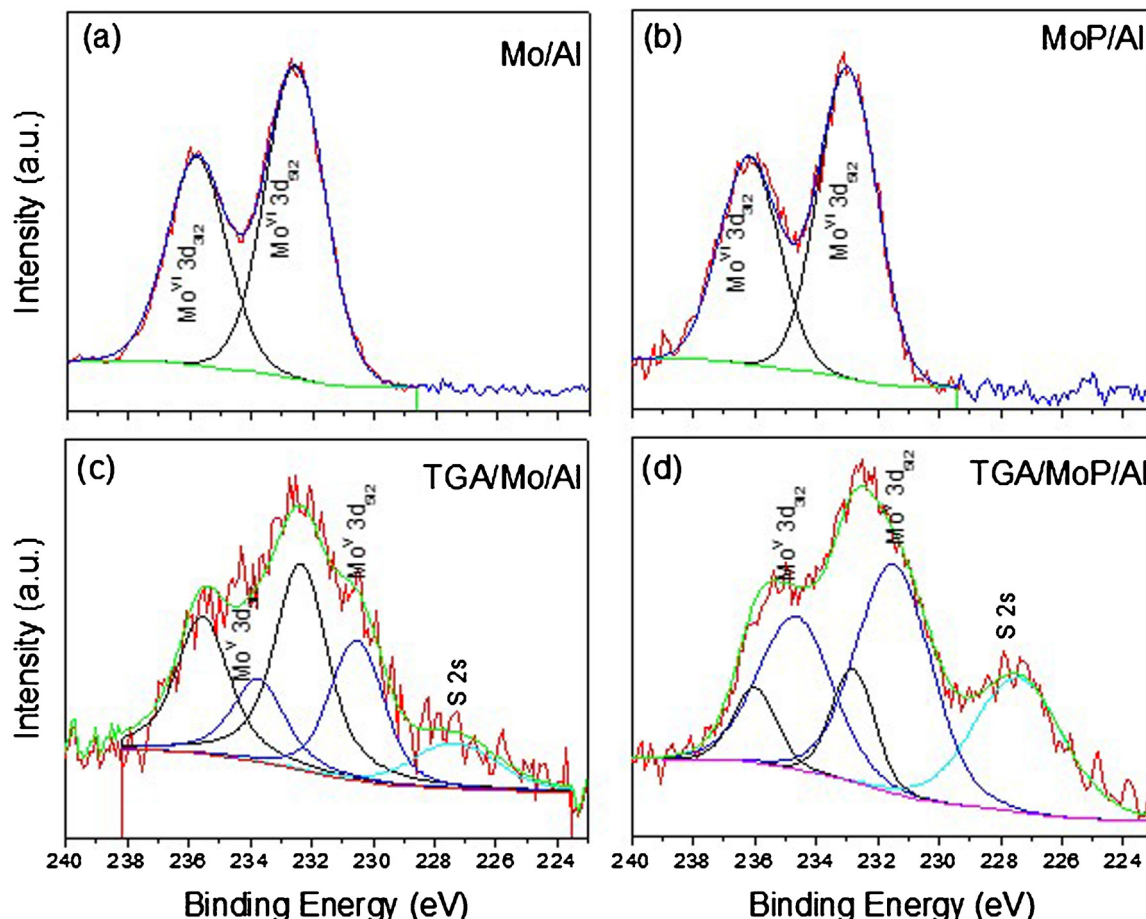


**Fig. 5.** XPS spectra of oxidic Mo/Al and MoP/Al catalysts prepared with and without TGA: (a) Mo/Al, (b) MoP/Al, (c) TGA/Mo/Al and (d) TGA/MoP/Al.

**Table 3**

Binding energy values for surface Al, Mo, and S species over various sulfided catalysts, from analysis and deconvolution of XPS data of Fig. 6. Full-width at half maximum (FWHM) values of various signals also included (between parentheses).  $Mo_T = Mo^{VI} + Mo^V + Mo^{VI}$ .

Sample/ signal assigning	Al 2p	MoVI 3d <sub>5/2</sub>	MoV 3d <sub>5/2</sub>	MoIV 3d <sub>5/2</sub>	S 2p	MoIV/MoT
Mo/Al	74.2 (1.5)	232.3 (2.0)	229.6 (1.5)	228.8 (1.0)	161.7 (1.3)	0.44
MoP/Al	74.2 (1.8)	232.7 (1.9)	231.5 (2.2)	228.9 (1.6)	162.0 (3.4)	0.29
TGA/Mo/Al	74.3 (1.7)	232.7 (1.6)	231.0 (2.2)	228.8 (1.3)	161.7 (1.4)	0.43
TGA/MoP/Al	74.2 (1.8)	232.8 (2.2)	230.7 (2.1)	228.9 (1.5)	161.9 (1.8)	0.59

### 3.5. XPS analysis of sulfide catalysts

In the cases of sulfide catalysts, the Mo 3d signal was fitted to the following species: (i) Mo<sup>IV</sup> from sulfide MoS<sub>2</sub> (active species), (ii) Mo<sup>V</sup> from molybdenum oxy-sulfides and, (iii) Mo<sup>VI</sup> from un-reduced molybdenum oxide [33,34] (see Fig. 6). Corresponding XPS parameters of Mo species, Al 2p and S 2p are presented in Table 3. Mo<sup>IV</sup> represents the sulfide active species dispersed on alumina surface. In Mo/Al sample, where strong MoO<sub>x</sub> species-carrier interaction is expected, TGA addition did not modify the sulfidability, as a similar MoS<sub>2</sub> fraction was observed over both catalysts (0.43 and 0.44, respectively).

On the other hand, on MoP/Al where larger MoO<sub>x</sub> aggregates were identified (see section 3.2) and higher amount of LMCT com-

plexes were formed by TGA complexation (as discussed in section 3.3), a fraction of fully sulfide Mo was significantly higher (by a factor of 2) when using the organic modifier.

### 3.6. Characterization of oxidic catalysts precursors by HRTEM

HRTEM images of oxidic catalysts are shown in Fig. 7. For Mo/Al and MoP/Al samples, small patches of crystallites with atomic resolution from very dispersed MoO<sub>x</sub> species with a few atomic layers, were observed on the alumina surface (see Fig. 7a and b). With TGA addition, smaller than 1 nm nanoparticles smeared on the support surface together with MoO<sub>x</sub> species appeared (see Fig. 7c and d). These results suggest that TGA addition redistribute MoO<sub>x</sub> species lowering its interaction with the support.

### 3.7. Characterization of sulfide materials by HRTEM

MoS<sub>2</sub> structure in all samples after sulfidation procedure is shown in Fig. 8. Here, MoS<sub>2</sub> clusters oriented perpendicular to the direction of the electron beam on a thin layer of  $\gamma$ -Al<sub>2</sub>O<sub>3</sub> in HRTEM images were observed. The d-spacing of the stacked MoS<sub>2</sub> clusters was around 0.62 nm, very close to the (002) spacing of a MoS<sub>2</sub> crystal. The line spacing was taken between S-Mo-S layers because in bulk MoS<sub>2</sub> generally has a hexagonal system stacked in S-Mo-S layers along the c-axis. This S-Mo-S layered structure leads to two different bond types on the  $\gamma$ -Al<sub>2</sub>O<sub>3</sub> support surface. Basal plane, namely the (001) plane parallel to the S-Mo-S layers and edge planes (the (100) and (110) planes) perpendicular to the S-Mo-S layers. The MoS<sub>2</sub> clusters oriented perpendicular to

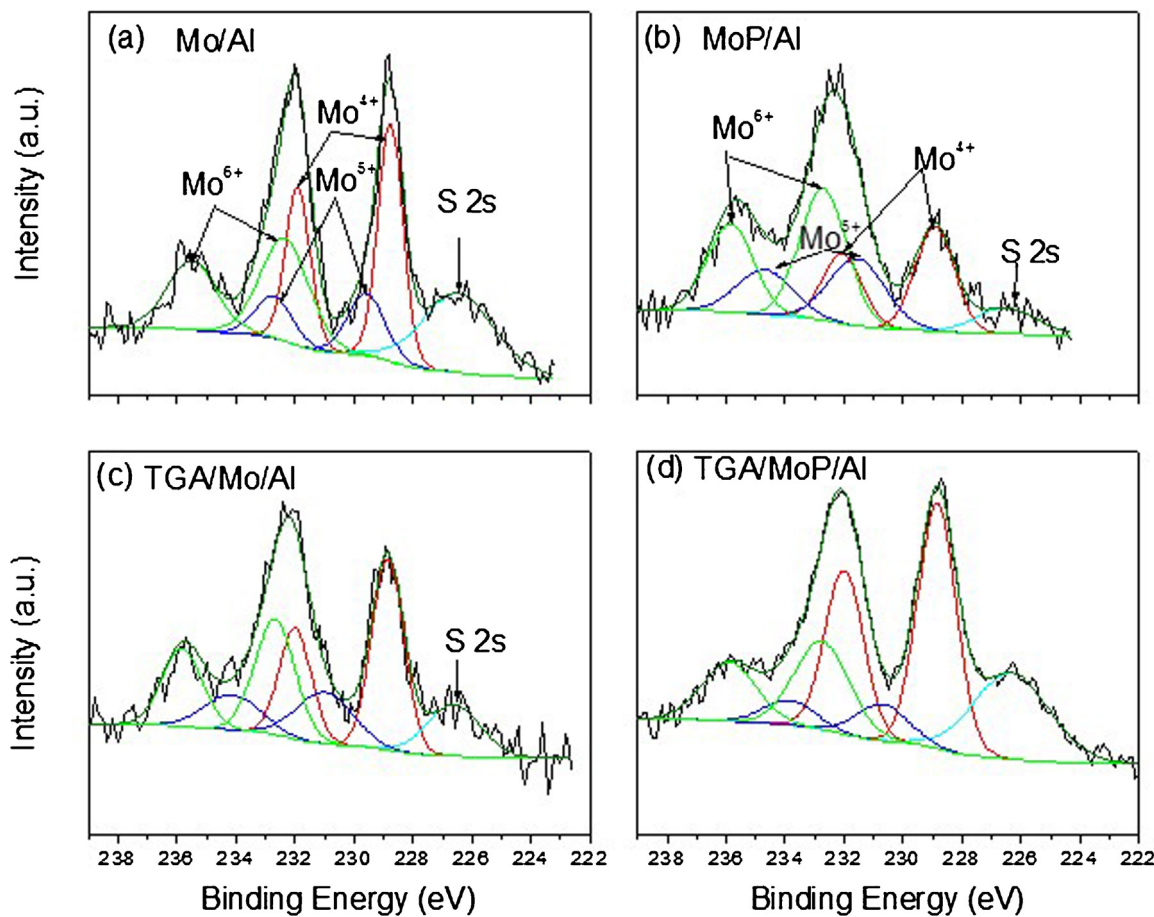


**Fig. 6.** XPS spectra of sulfided Mo/Al and MoP/Al catalysts prepared with and without TGA: (a) Mo/Al, (b) MoP/Al, (c) TGA/Mo/Al and (d) TGA/MoP/Al.

**Table 4**

Statistical distribution of (a) stacking and (b) length of MoS<sub>2</sub> slabs over various sulfided catalysts prepared from corresponding HRTEM micrographs of Fig. 7. Sulfided Mo dispersion also included.

Catalyst	Stacking	Slab length(nm)	D <sub>Mo</sub> <sup>a</sup>
Mo/Al	2.3 ± 0.5	3.8 ± 0.6	0.31
MoP/Al	2.5 ± 0.5	3.7 ± 1.4	0.32
TGA/Mo/Al	3.0 ± 0.7	3.9 ± 1.1	0.30
TGA/MoP/Al	2.9 ± 0.7	3.6 ± 0.6	0.32

<sup>a</sup> Calculated by using Mo<sup>IV</sup> dispersion as determined from Eq. (4).

the direction of the electron beam have been regarded as the active sites for HDS reactions, therefore, given their importance as active centers a statistic study of length and stacking number was carried out. Apparently, Phosphorous addition did not appreciably affect neither stacking nor slab length of corresponding sulfide catalysts (see images in Fig. 8), as in Mo/Al material (Table 4). On the other hand, a higher stacking was evident in both TGA-modified formulations. However, MoS<sub>2</sub> layers length remained essentially unaltered. Statistical distribution of stacking and slab length over different formulations was plotted in Fig. 9. Dispersion of Mo atoms in MoS<sub>2</sub> crystals was determined by geometrical model from Kasztelan et al. [35]. Thus,

$$D_{Mo} = \frac{Mo_e + Mo_c}{Mo_t} = \frac{\sum_{i=1 \dots t} 6n_i - 6}{\sum_{i=1 \dots t} 3n_i^2 - n_i - 1} \quad (4)$$

where D<sub>Mo</sub> is MoS<sub>2</sub> dispersion, Mo<sub>e</sub>, Mo<sub>c</sub> and Mo<sub>t</sub> are Mo atoms on the edges, corners and total ones (as determined by slabs size);

n<sub>i</sub> is the number of atoms along one side of a Mo sulfide slab (as determined from its length) and t is the total number of slabs analyzed from HRTEM corresponding micrographs during the statistical counting.

No significant differences were observed for Mo sulfide dispersion on our catalysts as indicated in Table 4. Then, the main effect of TGA addition is likely related to a higher stacking (ca. 30%) in the formulation prepared without P. This result may be attributed to a weak oxidic Mo-alumina interaction due to formation of chelating complexes between Mo species and TGA through –SH and –COOH moieties [28,31,36]. Additionally, strong structural modifications in the MoS<sub>2</sub> clusters were observed with TGA addition. Annular dark field (ADF) images of single MoS<sub>2</sub> clusters observed on the basal plane (see inset Fourier Transform) are shown in Fig. 10, where the hexagonal arrangement of the Mo atoms was revealed. A MoS<sub>2</sub> crystal, free of structural defects, is shown in ADF image of the sample without TGA (see Fig. 10a). Here, only atomic steps and terraces produced by S-Mo-S layers of different sizes stacked on basal plane, were observed. Brighter Mo atom regions indicate more S-Mo-S layers on the basal plane in ADF image. When the TGA was added, clear changes in the structure of the MoS<sub>2</sub> crystal were produced (see Fig. 10b), that is, a large area of single-layered MoS<sub>2</sub> cluster basal-bonded to the support. Several vacant sites of Mo atoms on the S-Mo-S layer can be noted. The lack of Mo atoms generated a distortion in the lattice. Vacant sites and atomic steps generate a larger amount of catalytically active sites for HDS reactions, as will be examined in the following section.

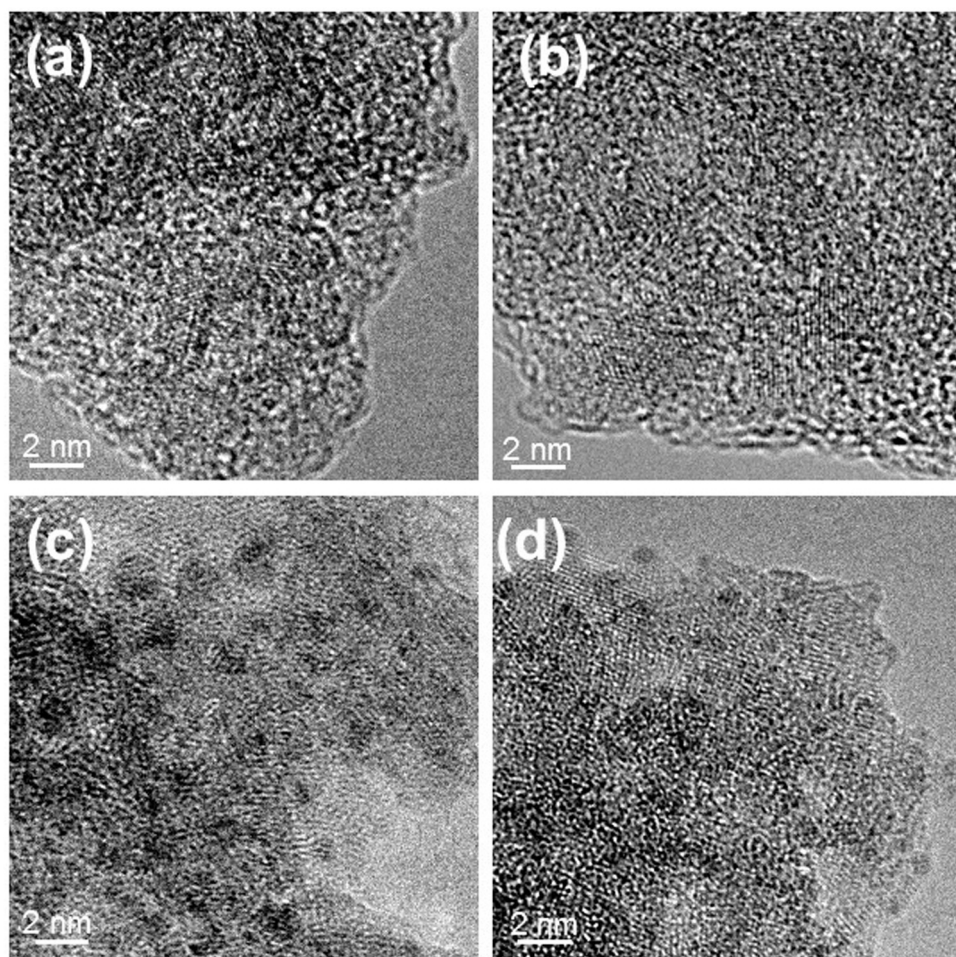


**Fig. 7.** HRTEM images of the  $\text{MoO}_x$  species on thin film regions of the  $\text{Al}_2\text{O}_3$  support of: (a) Mo/Al, (b) MoP/Al, (c) TGA/Mo/Al and (d) TGA/MoP/Al.

### 3.8. Catalytic activity test (dibenzothiophene hydrodesulfurization)

Pseudo-first order kinetic constants in the liquid-phase DBT HDS on various sulfided catalysts are shown in Table 5, where corresponding values were expressed on intrinsic (considering Mo loading) and per mass of  $\text{MoS}_2$  basis. Considering the latter basis, Mo/Al HDS activity increased two-fold by P addition. Moreover, TGA modification contributed to get improved HDS properties although in a much lower degree (~20% enhancement). According to Nicosia and Prins, in the case of glycol-modified CoMo/ $\text{Al}_2\text{O}_3$  sulfided catalysts [37], a combined simultaneous influence of P and the organic additive TGA was remarkable, where a four-fold higher activity was observed for TGA/MoP/Al, compared to that of MoP/Al. The observed activity trend was similar on a per active sites basis (see fourth column of Table 5).

The very high activity of TGA/MoP/Al catalyst points out to the creation of  $\text{MoS}_2$  sites of much higher intrinsic activity as to those over the material prepared with no organic additive. Weak Mo-support interaction due to the effect of TGA addition strongly suggest the formation of fully sulfide Type II sites [38] whose activity is two-fold as to that of the conventional Type I ones, which are in stronger interaction with alumina carrier. In the case of Type I sites, stable Mo-O-Al bonds in the crystallites in direct contact with  $\text{Al}_2\text{O}_3$  [39–43] cannot be broken by sulfiding under conditions commonly used during HDS catalyst activation, limiting the S-removal activity of resulting  $\text{MoS}_2$  particles. Conversely, in fully sulfide Type II catalysts the interaction of supported  $\text{MoS}_2$  particles-carrier is due to

weak van der Waals forces. On the other hand, in the case of Mo/Al prepared without phosphorus, too strong interactions between the alumina carrier and deposited oxidic Mo species might hinder efficient transformation of Type I sites to preferred Type II ones of enhanced HDS activity.

In order to explain catalytic performance results, we must refer to the corresponding characterization results of previous sections. From UV-vis and Raman spectroscopy results, very strong interaction between polymolybdate species and alumina carrier was established in Mo/Al sample, whereas with phosphorus addition together with the highly disperse polymolybdate species, larger aggregates of  $\text{MoO}_3$  were detected on alumina surface. With TGA addition, Mo-TGA complexes formed in both Mo/Al and MoP/Al samples, but a lower degree of reduction of  $\text{Mo}^{\text{VI}}$  to  $\text{Mo}^{\text{V}}$  was estimated by XPS on the sample where Mo species are in strong interaction with the support; whereas in a sample with large aggregate of  $\text{MoO}_3$  (MoP/Al) the  $\text{Mo}^{\text{VI}}$  was reduced more efficiently (twice as much). These results suggests that TGA react with  $\text{MoO}_3$  aggregates yielding LMCT complexes more efficiently than with highly dispersed polymolybdates species in strong interaction with the support. Therefore, these results point out that TGA redissolve and redisperse the  $\text{MoO}_3$  on the alumina surface via complexation, such as reported elsewhere by addition of polyethylene glycol on oxidic industrial HDS catalysts [22]. In fact, addition of oxygen containing compounds are a common practice on the reactivation/rejuvenation treatment playing a role as chelating agents and thus helping to redissolve and redisperse the metals [16].

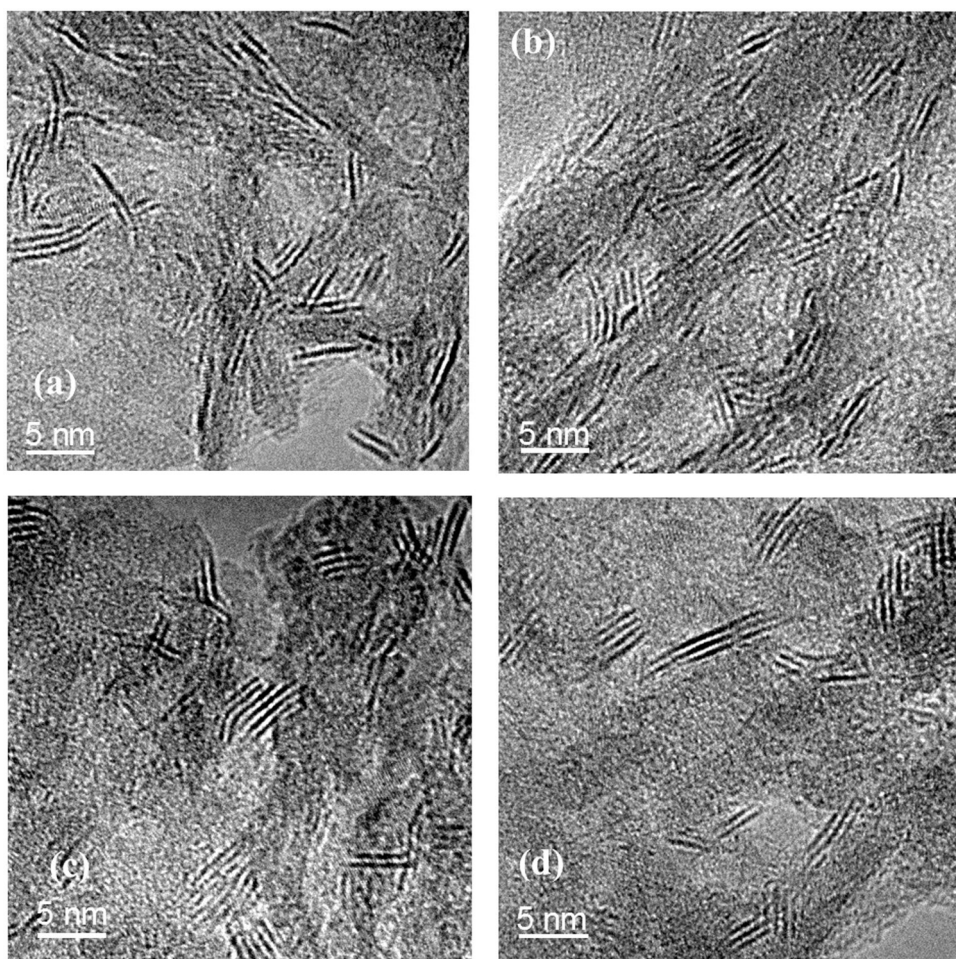


**Fig. 8.** HRTEM images showing the MoS<sub>2</sub> clusters oriented perpendicular to the direction of the electron beam on thin film regions of the Al<sub>2</sub>O<sub>3</sub> support of: (a) Mo/Al, (b) MoP/Al, (c) TGA/Mo/Al and (d) TGA/MoP/Al. The S-Mo-S layers perpendicular to the edge planes can be clearly appreciated.

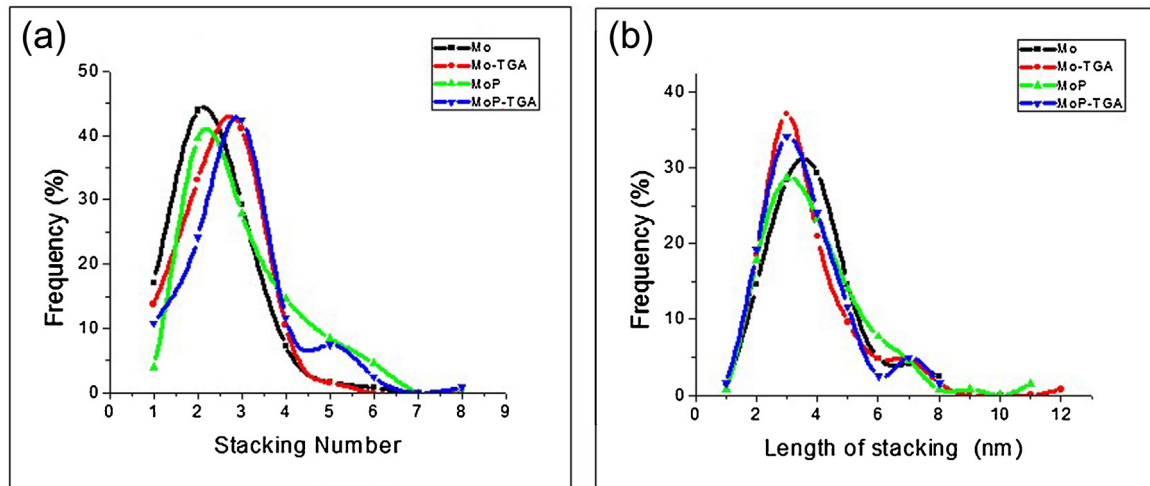


**Fig. 9.** Statistical distribution of: (a) stacking and (b) length of MoS<sub>2</sub> slabs over various sulfided catalysts prepared from corresponding HRTEM micrographs of Fig. 7. Sulfided Mo dispersion also included.

During the activation process, sulfidation degree of MoO<sub>x</sub> species in strong interaction with the support (Mo/Al sample) remains constant at Mo<sup>IV</sup>/Mo<sub>T</sub> surface atomic ratio of 0.4, regardless of the addition of TGA (see last column in Table 3). In the case of MoP/Al sample, where large MoO<sub>3</sub> aggregates were detected, addition of TGA brought about a considerable increase (twice as

much) in sulfidation degree, in comparison with counterpart without TGA. These results confirm that TGA contributes to a higher sulfidation and dispersion of active MoS<sub>2</sub> phase by a complexation of MoO<sub>3</sub> aggregated particles redissolving/redispersing Mo species which increase the density of active phase on the carrier surface, and generate fully sulfide Type II sites [38]. However, when strong

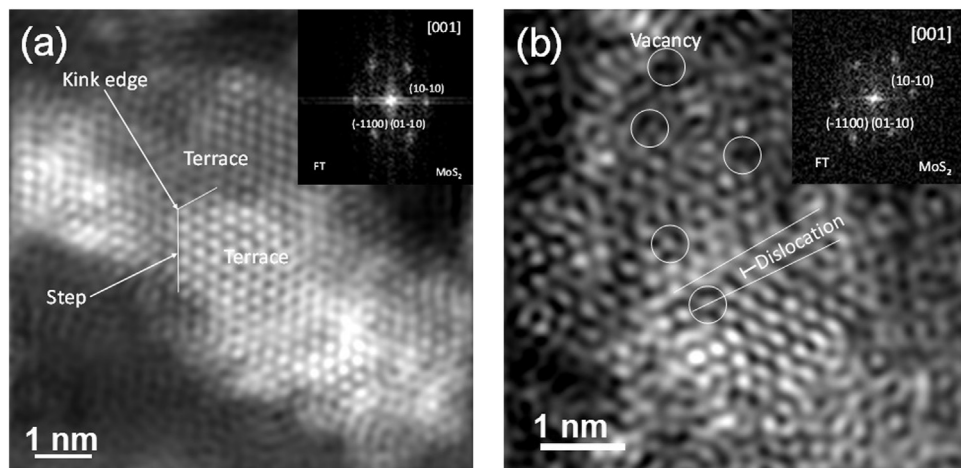


**Fig. 10.** Annular Dark Field images showing the Mo atomic column positions in a MoS<sub>2</sub> crystal viewed along the [0001] direction: (a) MoP/Al and (b) TGA/MoP/Al sulfided catalysts.

**Table 5**

Pseudo first order intrinsic kinetic constant values in DBT-HDS over sulfided catalysts prepared with and without TGA.

Catalyst	$k \times 10^{-6}$ (l/(g <sub>Mo</sub> s))	<sup>a</sup> $k' \times 10^{-6}$ (l/(g <sub>MoS2</sub> s))	<sup>b</sup> $k'' \times 10^{-28}$ (l/(at <sub>(Mo+MoC)</sub> s))	<sup>c</sup> $S_{THDBT}$ (%)	<sup>c</sup> $S_{BP}$ (%)	<sup>c</sup> $S_{CHB}$ (%)	<sup>c</sup> $S_{DDS}/S_{HYD}$
Mo/Al	0.57	1.30	6.66	11	47	42	0.89
MoP/Al	0.73	2.52	12.54	21	47	32	0.89
TGA/Mo/Al	0.67	1.56	8.27	14	39	47	0.64
TGA/MoP/Al	3.00	5.08	25.31	14	54	32	1.17

<sup>a</sup> Calculated by using Mo<sup>IV</sup> fraction as determined by XPS analysis (from Table 3).

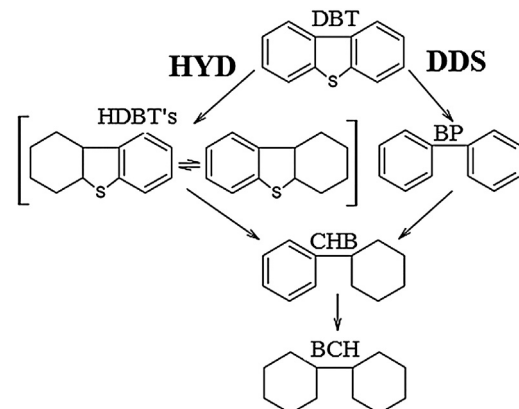
<sup>b</sup> Calculated by using Mo<sup>IV</sup> dispersion as determined from Eq. (4).

<sup>c</sup> At ~30% DBT conversion.

interaction takes place between MoO<sub>x</sub> species and alumina surface (Mo/Al sample), TGA did not affect this interaction and sulfidation degree remained constant, since stable Mo-O-Al bonds in the crystallites are in direct contact with Al<sub>2</sub>O<sub>3</sub> [39–43], and TGA cannot break these bonds and then Type I sites are favored.

HDS activity showed a correlated behavior, that is, in Mo/Al sample with Type I sites, little enhancement on intrinsic kinetic constant was observed with TGA addition, indicating that TGA did not change the nature of active sites. In the case of MoP/sample, with Type II sites, HDS activity was as twice as that of the conventional type I ones on Mo/Al sample, and addition of TGA increased the dispersion of these Type II sites and HDS activity increased twofold.

Among HDS reaction products, biphenyl (BP, from direct desulfurization route, DDS [44]) and tetrahydrodibenzothiophene and cyclohexylbenzene (THDBT and CHB respectively, species from the hydrogenation, HYD, pathway) were identified (see Scheme 1 [45] and Fig. 11). The phosphorus addition did not alter the  $S_{DDS}/S_{HYD}$  ratio in agreement with similar MoS<sub>2</sub> morphology over both sulfide catalysts (see Table 5). However, higher Mo sulfide slabs stacking produced by TGA modification (see Table 5) significantly affected the reaction routes, but in opposite ways, depending on the presence or absence of phosphorus in the formulation. Depending on the different nature of active sites generated on the surface, as mentioned above, TGA addition on MoO<sub>x</sub> in strong interaction with alumina (Mo/Al sample) did not modify the Type I sites, whereas TGA addition on large MoO<sub>3</sub> aggregates (MoP/Al sample) redisperses the active component and generates Type II catalysts with high amount of vacant sites and atomic steps (see HRTEM results, Fig. 10b) that favors HDS reactions via the DDS route. Additionally, more stacked MoS<sub>2</sub> particles over TGA/MoP/Al efficiently promoted DBT conversion through the DDS route, in agreement with Shimada [46] and Daage and Chianelli [47] in their so-called “rim-edge



**Scheme 1.** DBT HDS reaction network over sulphided CoMo/Al<sub>2</sub>O<sub>3</sub> (from reference 45).

model” of unsupported MoS<sub>2</sub> catalysts tested in DBT HDS. Other authors [17,19] have also found increased contribution of DDS route in HDS tests of TGA-modified promoted MoS<sub>2</sub> catalysts where differently to our case, improved production of ethylbenzene (from benzothiophene via DDS reaction pathway) was attributed to preferred formation of the highly active “NiMoS” phase characterized by its good performance in direct sulfur extrusion.

#### 4. Conclusions

Alumina-supported Mo-based hydrodesulfurization catalysts (14 wt% Mo loading) were modified using chelating thioglycolic acid (TGA, TGA/Mo = 1 mol ratio), added by pore filling impregnation. Ligand to metal charge transfer (LMCT) complexes between TGA and Mo atoms, where partially reduced Mo<sup>5+</sup> species were

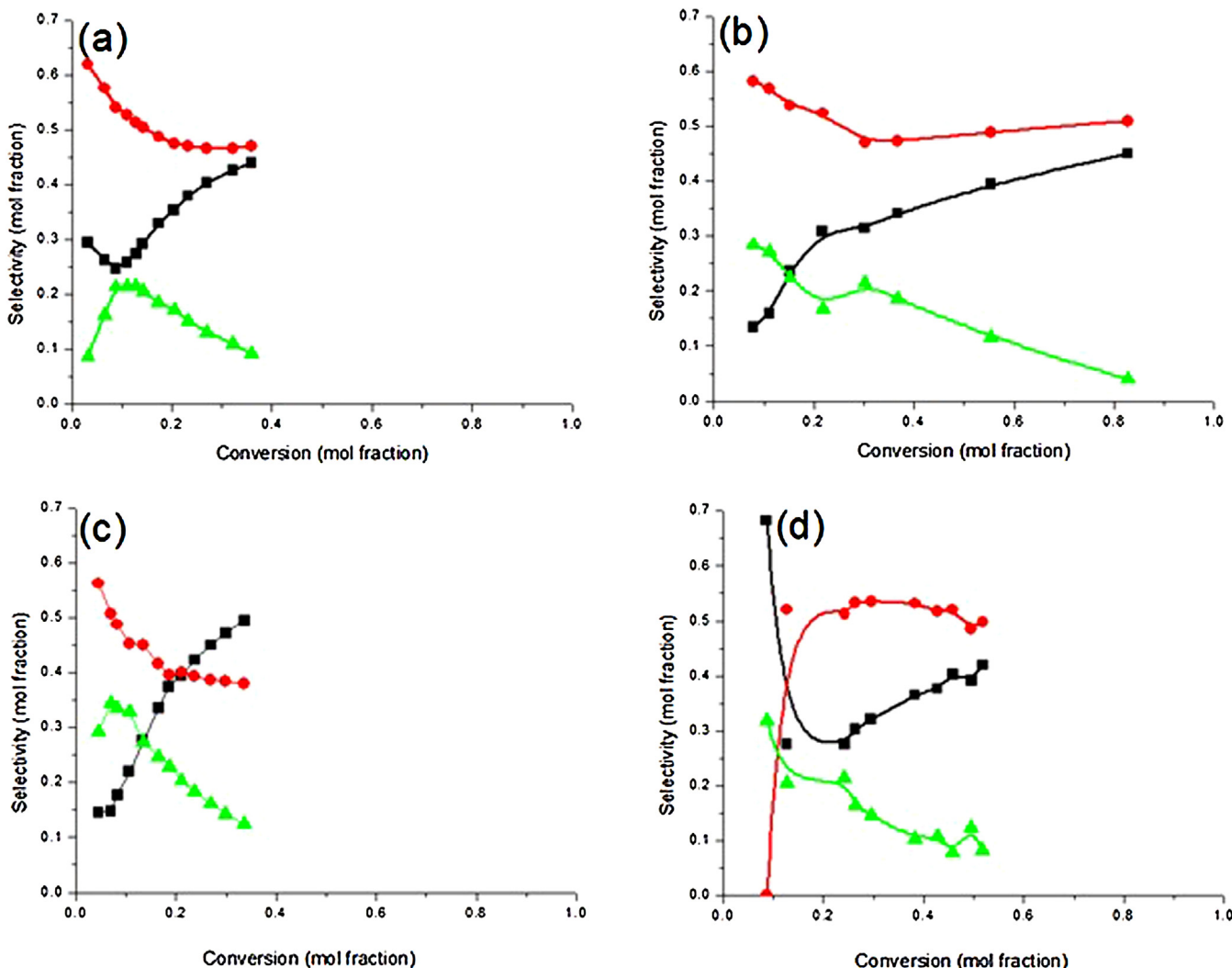


**Fig. 11.** DBT HDS and selectivity to various products over various prepared materials. (a): Mo/Al; (b): MoP/Al; (c): TGA/Mo/Al; (d): TGA/MoP/Al. ▲: Tetrahydrodibenzothiophene; ●: Biphenyl; ■: Cyclohexylbenzene.

detected (by XPS), were correlated to electronic transitions bands in the UV-vis region of corresponding spectra. Additionally, the catalysts prepared from phosphomolybdates impregnation of TGA resulted in two-fold increase of  $\text{Mo}^{4+}$  sulfide species as determined by XPS. TGA impregnation resulted in materials with increased stacking of  $\text{MoS}_2$  slabs with length essentially unaltered. Highly active (as tested in liquid-phase dibenzothiophene hydrodesulfurization) Type II sites formation was strongly suggested in sulfide TGA-modified formulations. Increased selectivity to biphenyl from direct desulfurization route over these catalysts was related to higher stacking of Mo sulfide particles. TGA promotes a higher sulfidation of active  $\text{MoS}_2$  phase by a complexation of  $\text{MoO}_x$  particles by redissolving/redispersing Mo species which increase the density of active phase on the carrier surface, and generate fully sulfided Type II sites.

## Acknowledgements

This work was funded by SENER-CONACYT project 116003 and IMP project Y.00103 and D.00447. Authors thank to “Centro de nanociencias y Micro y Nanotecnologías of Instituto Politécnico Nacional” for access to the Electron Microscopy Facilities and assistance in the operation in STEM mode of the JEOL ARM200CF.

## References

- [1] S. Badoga, K. Chandra Mouli, K.K. Soni, A.K. Dalai, J. Adjaye, *Appl. Catal. B: Env.* 125 (2012) 67–84.
- [2] Y. Ohta, T. Shimizu, T. Honma, M. Yamada, *Stud. Surf. Sci. Catal.* 127 (1999) 161–168.
- [3] M. Sun, D. Nicosia, R. Prins, *Catal. Today* 86 (2003) 173–189.
- [4] L. Peña, D. Valencia, T. Klimova, *Appl. Catal. B: Env.* 147 (2014) 879–887.
- [5] M.S. Rana, J. Ramírez, A. Gutiérrez-Alejandro, J. Ancheyta, L. Cedeño, S.K. Maity, *J. Catal.* 246 (2007) 100–108.
- [6] L. Kaluza, D. Gulkova, Z. Vit, M. Zdráhal, *Catal. Lett.* 142 (2012) 969–974.
- [7] M.A. Lélias, P.J. Kooyman, L. Mariey, L. Oliviero, A. Travert, J. van Gestel, J.A.R. van Veen, F. Maugé, *J. Catal.* 267 (2009) 14–23.
- [8] J. Escobar, M.C. Barrera, J.A. de los Reyes, J.A. Toledo, V. Santés, J.A. Colín, *J. Mol. Catal. A: Chem.* 287 (2008) 33–40.
- [9] D. Valencia, T. Klimova, *Appl. Catal. B: Env.* 129 (2013) 137–145.
- [10] L. van Handel, G.M. Bremmer, E.J.M. Hensen, Th. Weber, *J. Catal.* 342 (2016) 27–39.
- [11] C. Galsson, C. Geantet, M. Lacroix, F. Labruyere, P. Dufresne, *J. Catal.* 212 (2002) 76–85.
- [12] J. Vangestel, J. Leglise, J.C. Duchet, *J. Catal.* 145 (2) (1994) 429–436.
- [13] P. Dufresne, N. Brahma, F. Labruyere, M. Lacroix, M. Breysse, *Catal. Today* 29 (1996) 251–254.
- [14] F. Labruyere, P. Dufresne, M. Lacroix, M. Breysse, *Catal. Today* 43 (1998) 111–116.
- [15] J.H. Wilson, G. Berrebi, *Stud. Surf. Sci. Catal.* 38 (1988) 393–398.
- [16] P. Dufresne, *Appl. Catal. A: Gen.* 322 (2007) 67–75.
- [17] N. Frizi, P. Blanchard, E. Payen, P. Baranek, C. Lancelot, M. Rebeilleau, C. Dupuy, J.P. Dath, *Catal. Today* 130 (2008) 32–40.
- [18] N. Frizi, P. Blanchard, E. Payen, P. Baranek, M. Rebeilleau, C. Dupuy, J.P. Dath, *Catal. Today* 130 (2008) 272–282.

- [19] R. Palcheva, L. Kaluža, L. Dimitrov, G. Tyuliev, *Appl. Catal. A* 520 (2016) 24–34.
- [20] R.A. Ortega-Domínguez, J.A. Mendoza-Nieto, P. Hernández-Hipólito, F. Garrido-Sánchez, J. Escobar-Aguilar, S.A.I. Barri, D. Chadwick, T.E. Klimova, *J. Catal.* 329 (2015) 457–470.
- [21] Y. Saito, M. Nagata, T. Funamoto, Y. Masuyama, K. Segawa, *Appl. Catal. A* 295 (2005) 11–22.
- [22] J. Ramírez, L. Cedeño, G. Busca, *J. Catal.* 184 (1999) 59–67.
- [23] G. Mestl, T.K.K. Srinivasan, *Catal. Rev. Sci. Eng.* 40 (1998) 451–570.
- [24] B.L. Mojet, L. Coulier, J. van Grondelle, J.W. Niemantsverdriet, R.A. van Santen, *Catal. Lett.* 96 (2004) 1–4.
- [25] M. Dieterle, G. Weinberg, G. Mestl, *Phys. Chem. Chem. Phys.* 4 (2002) 812–821.
- [26] M. de Boer, A.J. van Dillen, D.C. Koningsberger, J.W. Geus, M.A. Vuurman, I.E. Wachs, *Catal. Letters* 11 (1991) 227–240.
- [27] M. Brandhorst, S. Cristol, M. Capron, C. Dujardin, H. Vezin, G. Le Bourdon, E. Payen, *Catal. Today* 113 (2006) 34–39.
- [28] A. Cervilla, E. Llopis, A. Doménech, A. Ribera, P. Palanca, P. Gómez-Romero, *J. Chem. Soc. Dalton Trans.* 6 (1992) 1005–1008.
- [29] H. Aritani, T. Tanaka, T. Funabiki, S. Yoshida, K. Eda, N. Sotani, M. Kudo, S. Hasegawa, *J. Phys. Chem.* 100 (1996) 19495–19501.
- [30] P.C.H. Mitchell, *Coord. Chem. Rev.* 1 (1966) 315–350.
- [31] J.F. Martin, J.T. Spence, *J. Phys. Chem.* 74 (1970) 3589–3596.
- [32] W. Yang, C. Lu, S. Lu, H. Zhuang, *Helvet. Chim. Acta* 85 (2002) 2417–2429.
- [33] J.C. Muijsers, Th. Weber, V. van Hardeveld, H.W. Zandbergen, J.W. Niemantsverdriet, *J. Catal.* 157 (1995) 698–705.
- [34] Th. Weber, J.C. Muijsers, J.H.M.C. van Wolput, C.P.J. Verhagen, J.W. Niemantsverdriet, *J. Phys. Chem.* 100 (1996) 14144–14150.
- [35] S. Kasztelan, H. Toulhoat, J. Grimblot, J.P. Bonnelle, *Appl. Catal.* 13 (1984) 127–159.
- [36] A. Cervilla, A. Llopis, J.A. Ramírez, A. Doménech, P. Palanca, M.T. Pilcher, C.A. Guilardi, A. Orlandini, *J. Chem. Soc. Dalton Trans.* (1994) 175–183.
- [37] D. Nicosia, R. Prins, *J. Catal.* 229 (2005) 424–438.
- [38] R. Candia, J. Villadsen, N.-Y. Topsøe, B.S. Clausen, H. Topsøe, *Bull. Soc. Chim. Belg.* 93 (1984) 763–773.
- [39] R.G. Leliveld, A.J. van Dillen, J.W. Geus, D.C. Koningsberger, *J. Catal.* 165 (1997) 184–196.
- [40] N.-Y. Topsøe, H. Topsøe, *J. Catal.* 139 (1993) 540–631.
- [41] E.G. Derouane, E. Pedersen, B.S. Clausen, Z. Gabelica, R. Candia, H. Topsøe, *J. Catal.* 99 (1986) 253–261.
- [42] E.J.M. Hensen, V.H.J. De Beer, J.A.R. van Veen, R.A. van Santen, *Catal. Lett.* 84 (2002) 59.
- [43] E. Diemann, Th. Weber, A. Müller, *J. Catal.* 148 (1994) 288–303.
- [44] F. Bataille, J.L. Lemberton, P. Michaud, G. Pérrot, M. Vrnat, M. Lemaire, E. Schulz, M. Breysse, S. Kasztelan, *J. Catal.* 191 (2000) 409–422.
- [45] M. Houalla, N.K. Nag, A.V. Sapre, D.H. Broderick, B.C. Gates, *AIChE J.* 24 (1978) 1015–1021.
- [46] H. Shimada, *J. Jpn. Petrol. Inst.* 59 (2016) 46–58.
- [47] M. Daage, R. Chianelli, *J. Catal.* 149 (1994) 414–427.